COMMUNICATION

Rationally Designed, Three-Dimensional Carbon Nanotube Back-Contacts for Efficient Solar Devices

*Cary L. Pint, Kuniharu Takei, Rehan Kapadia, Maxwell Zheng, Alexandra C. Ford, Junjun Zhang, Arash Jamshidi, Rizia Bardhan, Jeffrey J. Urban, Ming Wu, Joel W. Ager, Michael M. Oye, and Ali Javey**

Devices designed to convert sunlight into usable sources of energy have become the focus of increased attention in the past decade due to the diminishing nature of fossil fuel resources.[1] As a result, recent research efforts have focused on improving solar device performance and cost using novel processes, materials and device technologies.[2,3] One example includes the use of three-dimensional (3-D) architectures to enhance the carrier collection efficiency and photon management of the devices.[4–6] In such a device concept, the efficiency of thin film solar devices can be enhanced by orthogonalizing the light absorption and carrier collection processes, especially for the material systems that exhibit low minority carrier lifetimes.[7] In addition, surface reflectance is reduced and the absorption is enhanced, thus improving the overall conversion efficiency. One route for fabricating 3-D solar devices involves the use of textured substrates and/or back-contacts followed by the conformal deposition of thin films of the absorber material.[8] In this regard, exploring scalable and tunable nanotexturing processes with high-aspect ratio features is required.

Here, we demonstrate the fabrication of textured carbon nanofiber (CNF) arrays for the back-contact of solar devices with improved photon capture properties. Using a scalable, solution-phase condensation process,[9–11] conductive and chemically robust CNF scaffolds with tunable pitch and feature shape/size are obtained. To explore the utility of the proposed approach, the nanotextured CNF electrodes are coated with conformal thin films of TiO_2 absorber layer for water oxidation.[12–17] Unlike the use of other reported TiO_2/CNF architectures, or nanotubes and nanowires made of TiO_2,[18–23] this morphology allows us to design antireflective absorbing layers to decouple and optimize absorption and carrier collection. Based upon this, we demonstrate an enhancement of up to 3 times in the short circuit current density (J_{SC}) for the 3-D CNF/TiO_2 photoelectrochemical (PEC) device as compared to its planar counterpart. Antireflection is particularly important as it is not feasible to use conventional antireflective coatings in PEC cells since the effective junction is formed at the semiconductor-liquid interface.[24] Such a coating would inhibit the injection of photo-generated minority carriers into the solution.

Figure 1 demonstrates the general fabrication approach for textured CNF back-contacts. First, vertically aligned CNF arrays (Figure 1a,c) are grown in a plasma-enhanced chemical vapor deposition system on Si/SiO_2 substrates using Ni catalyst thin films (thickness, 30 nm), supported on conductive Cu/Ti bilayers (thickness, 200/30 nm).[25] The fabricated CNF array is electrically addressable by the substrate and exhibits an average vertical height of ~10 μm and CNF diameters between 10-120 nm, as measured by SEM. Following the growth process, the vertically aligned CNF arrays are textured using a scalable solution-phase condensation process (Figure 1b,d).[9–11] Here, CNFs are exposed to a 20 μL drop of acetone (~0.6×0.6 cm^2 sample size) which is then dried under ambient conditions. Upon drying, capillary forces cause reorganization of the vertically aligned carbon nanofiber morphology, which is inherently dependent on the surface tension of the liquid.[9] Solvents with different surface tensions were found to yield variable structures upon drying, with acetone yielding the highest density of compact pillar structures with a base diameter of 4–5 μm (Figure 1d) that resulted in the most optimal device performance. The use of other solvents and drying conditions resulted in either larger pillars with smaller out-of-plane angles or else ridge-like pillars that formed cellular, interconnected structures. Therefore, acetone condensation was utilized throughout experiments described here.

Atomic layer deposition (ALD) at 250 °C was utilized to coat TiO_2 thin films with varied thicknesses (T_{TiO2} = 80–400 nm) on the surface of the texturized CNF templates as the light-absorbing material. As demonstrated in SEM images shown in

Dr. C. L. Pint, Dr. K. Takei, R. Kapadia, M. Zheng, A. C. Ford, J. Zhang, Prof. A. Javey
Department of Electrical Engineering and Computer Science
University of California, Berkeley
CA 94720 USA, Material Sciences Division
Lawrence Berkeley National Laboratory
Berkeley, CA 94720 USA
E-mail: ajavey@berkeley.edu
Dr. A. Jamshidi, Prof. M. Wu
Department of Electrical Engineering and Computer Science
University of California
Berkeley, CA 94720 USA
Dr. R. Bardhan, Dr. J. J. Urban
The Molecular Foundry
Material Sciences Division
Lawrence Berkeley National Laboratory
Berkeley, CA 94720 USA
Dr. J. W. Ager
Material Sciences Division
Lawrence Berkeley National Laboratory
Berkeley, CA 94720 USA
Dr. M. M. Oye
NASA Ames Research Center
Moffett Field, CA 94035, USA

DOI: 10.1002/aenm.201100436

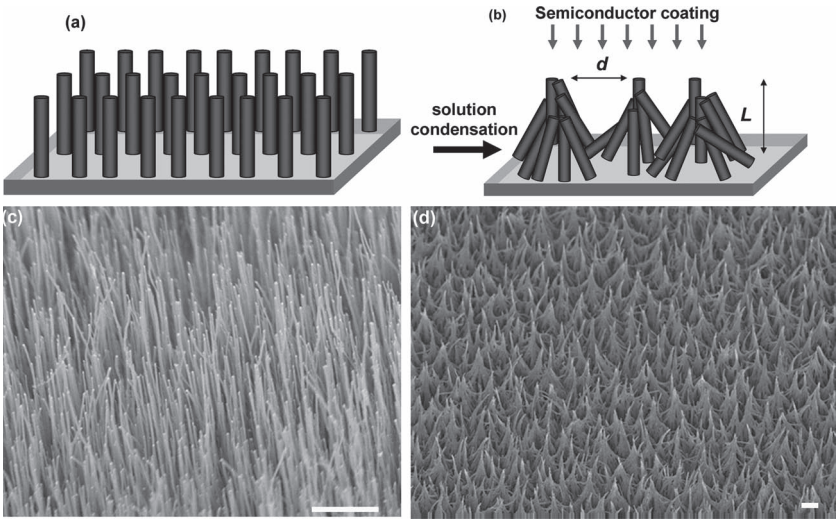

Figure 1. (a,b) Scheme of process depicting the capillary-force drying and texturizing of the as-grown carbon nanofiber arrays, (c) SEM image of as-grown carbon nanofiber array, and (d) SEM image of a texturized carbon nanofiber array. Scale bar in (c) and (d) is 3 μm.

Figure 2a–d, this TiO_2 coating is highly conformal. The TiO_2 thicknesses were confirmed for these structures by utilizing destructive SEM imaging (Figures 2c,d) where the pillars were intentionally broken to expose the conformal TiO_2 layer and the CNFs within. In order to determine the crystal structure of the TiO_2, x-ray diffraction (XRD) and Raman spectroscopy measurements were performed as shown in Figures 2e and 2f, respectively. From the XRD spectrum, the peaks labeled with "A" correspond to those of an ordered anatase phase of TiO_2 (body-centered cubic, I41/amd (141) JCPDS Card No. 108976). In addition, Raman spectroscopy depicts low frequency modes at ~147, 401, 520, and 639 cm^{-1} correlating well to the known modes of anatase TiO_2, also independently verifying the presence of anatase TiO_2.[26] It should be noted that anatase TiO_2 has a slightly higher band gap energy (3.2 eV) than other crystalline phases of TiO_2, but has also been suggested to be a more effective water oxidation photocatalyst.[27] Also, evident from the Raman spectrum are the broad and overlapping D and G bands centered around 1380 and 1600 cm^{-1}, respectively arising from the sp^3 hybridized graphitic structure of CNFs, similar to multi-walled nanotubes[28] (Figure 2(d)).

Figure 3b shows the current-potential curves for TiO_2/CNF structures with various T_{TiO2} utilizing an aqueous 1 M NaOH electrolyte solution. The measurements were taken under AM 1.5 G (1 sun) solar radiation using a three-electrode setup equipped with a Pt counter electrode and an Ag/AgCl reference electrode. AM 1.5 G illumination was utilized as a standard to compare the effect of electrode structure on the photocurrent generated by the TiO_2 absorber. As expected, the overall measured photocurrent is found to increase with increasing thickness for T_{TiO2} < ~300 nm due to enhanced absorption, with the greatest margin of increase in the thickness range of 80–220 nm. This range corresponds to 1-3 times the previously reported minority carrier diffusion length in TiO_2 (L_D~70–100 nm).[29,30] Beyond T_{TiO2}~300 nm (i.e., $T_{TiO2} > \sim 3\ L_D$), further increase in the thickness does not result in photocurrent enhancement since the generated carriers are mostly lost to recombination prior to reaching the surface.

In order to directly demonstrate the performance benefits of 3-D device architecture, we compare the measured J_{SC} of TiO_2/CNF structures to those of planar TiO_2/graphite devices. Here, J_{SC} for the three-electrode measurement is defined at the thermodynamic threshold voltage where the three-electrode cell has a net gain of free energy under illumination (0.216 V) based on the Nernst equation. The planar devices were made by the ALD of TiO_2 on a pressed graphite surface polished with 900 grit sandpaper and cleaned prior to coating. Shown in Figure 3c are the J_{SC} values for both the planar graphite and CNF templates as a function of T_{TiO2}. The 3-D TiO_2/CNF architecture consistently exhibits 2-3x enhancement in J_{SC} as compared to the planar devices with the same TiO_2 physical thickness.

We now consider factors that could contribute to the observed enhancement. These include (i) reduced surface reflectance, (ii) enhanced optical path length for the same TiO_2 physical thickness, and (iii) improved carrier collection efficiency. The reflectance of planar and 3-D textured samples can be directly assessed. Shown in **Figure 4**a is the percent reflectivity, R, as measured for the planar TiO_2/graphite substrate, and the coated texturized CNF templates. For both samples, T_{TiO2} ~ 60–80 nm. The reflectivity of the CNF templates is $R_{3\text{-}D}$ = 0.5-0.7% in the ultraviolet and visible regimes, whereas the reflectivity of the planar graphite is R_{planar} = 14–22%. Here, the effect of diffused light is ignored which can affect the absolute reflectance measured, but will not change the observed trend. The drastic low surface reflectance observed for 3D TiO_2 structures arises from the sub-wavelength tip-diameter, minimizing the interaction of light with the surface. An enhancement factor, γ, can be defined as $\gamma = (100\text{-}R_{3\text{-}D})/(100\text{-}R_{planar})$, which yields a suggested 1.2–1.3 times increase in device performance for the 3-D architecture based on minimized reflections. Given that conventional anti-reflective coating cannot be utilized in PEC devices, the use of a structural anti-reflective approach explored here is particularly important. Yet, reflectance alone does not explain the 2–3x enhancement in J_{SC} that is experimentally observed.

Next, we examine the effect of increased optical path[4,31–33] in textured CNF structures. The probability of a photogenerated carrier to diffuse to the semiconductor-electrolyte interface scales as $P \propto \exp\left(\frac{T_{TiO2}}{L_D}\right)$, suggesting that only the carriers generated within ~$3L_D$ of the surface contribute to J_{SC} with the rest mostly being lost to recombination processes. For TiO_2, given the previously reported L_D = 70–100 nm,[29,30] the maximum active thickness within which the carrier can be collected is hence only ~300nm. However, the optical characteristic length (~90% of all above-gap photons are absorbed) is on the order of 1 μm.[34] This suggests that structures that decouple the optical and carrier collection path lengths would result in enhanced device efficiencies. In this regard, CNF/TiO_2

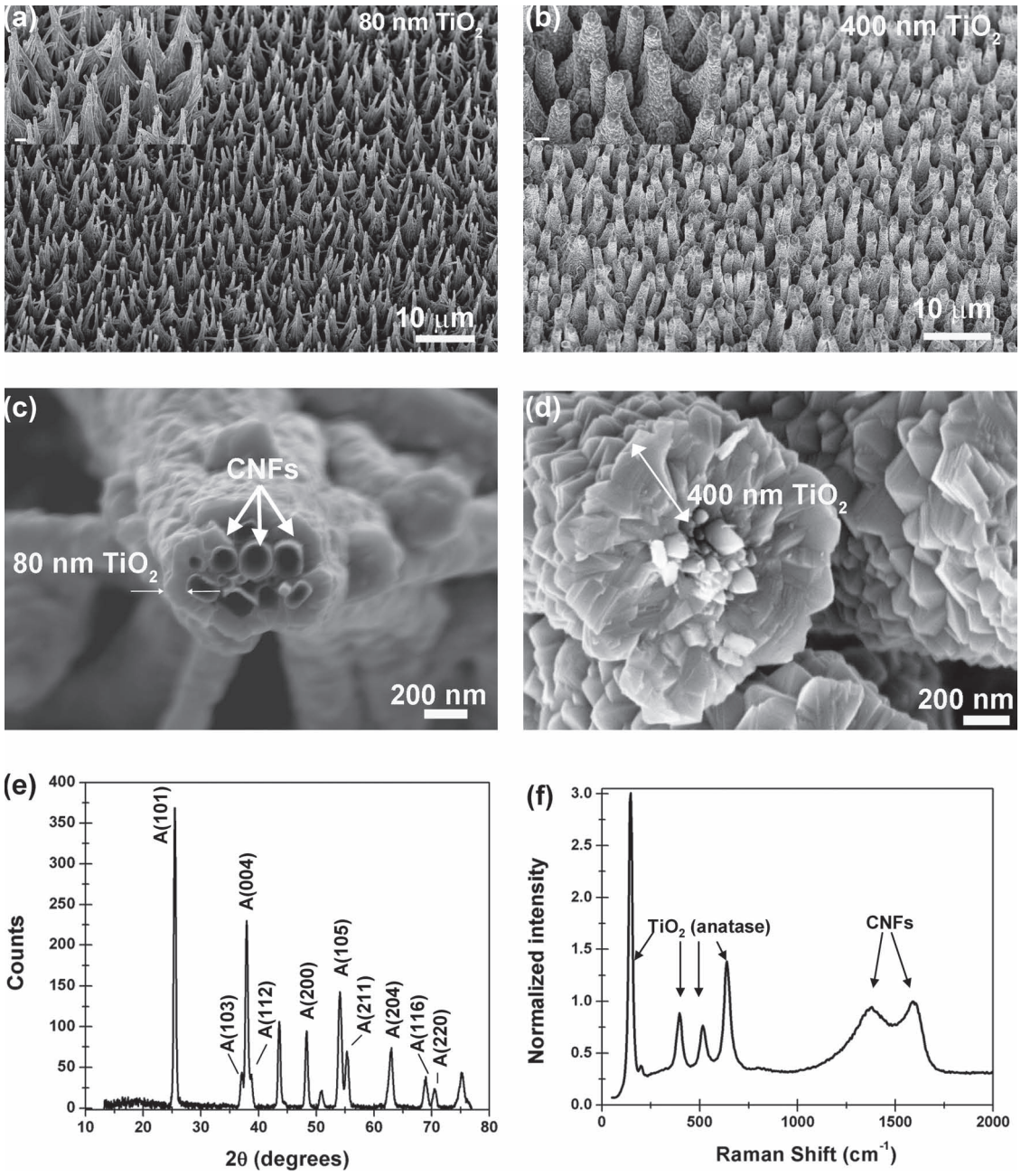

Figure 2. (a,b) SEM images of texturized carbon nanofiber arrays coated with (a) 80 nm TiO_2, and (b) 400 nm TiO_2. Inset in both images are higher magnification views. (c,d) Top-view SEM image of a broken TiO_2/CNF pillar with (c) 80 nm and (d) 400 nm TiO_2 coating. Characterization of TiO_2/CNF architectures using (e) XRD and (f) Raman spectroscopy to confirm the presence of anatase TiO_2 and the wall quality of the CNFs, respectively.

architecture explored here presents an advantage. A scheme depicting this mechanism is shown in Figure 4b. In this case, the high aspect-ratio structure inherent in the textured CNF electrodes results in the formation of a semiconductor absorber with a normal vector (along the direction of the thickness) oriented with some angle >60° relative to the average angle of incident radiation. This means that the effective thickness of the semiconductor is significantly greater than the actual physical thickness meaning that many more photons will be absorbed closer to a point where they can be collected.

The average out-of-plane angle of the textured CNFs (1–2 μm structure base radius, 10 μm height) explored here is $\theta = 75°–85°$ on average based on SEM characterization (Figure S1). For ideal normal incident radiation, geometrical considerations suggest a structure with $\theta \sim 80°$ to yield ~ 6x enhancement in the optical path length as compared to the physical material thickness. This means for $T_{TiO2} = 300$ nm ~ $3L_D$, an optical path length of ~1.8 μm can be achieved for the normal incident light. In actuality, this simple geometric consideration considerably overestimates the enhancement factor since it assumes only an

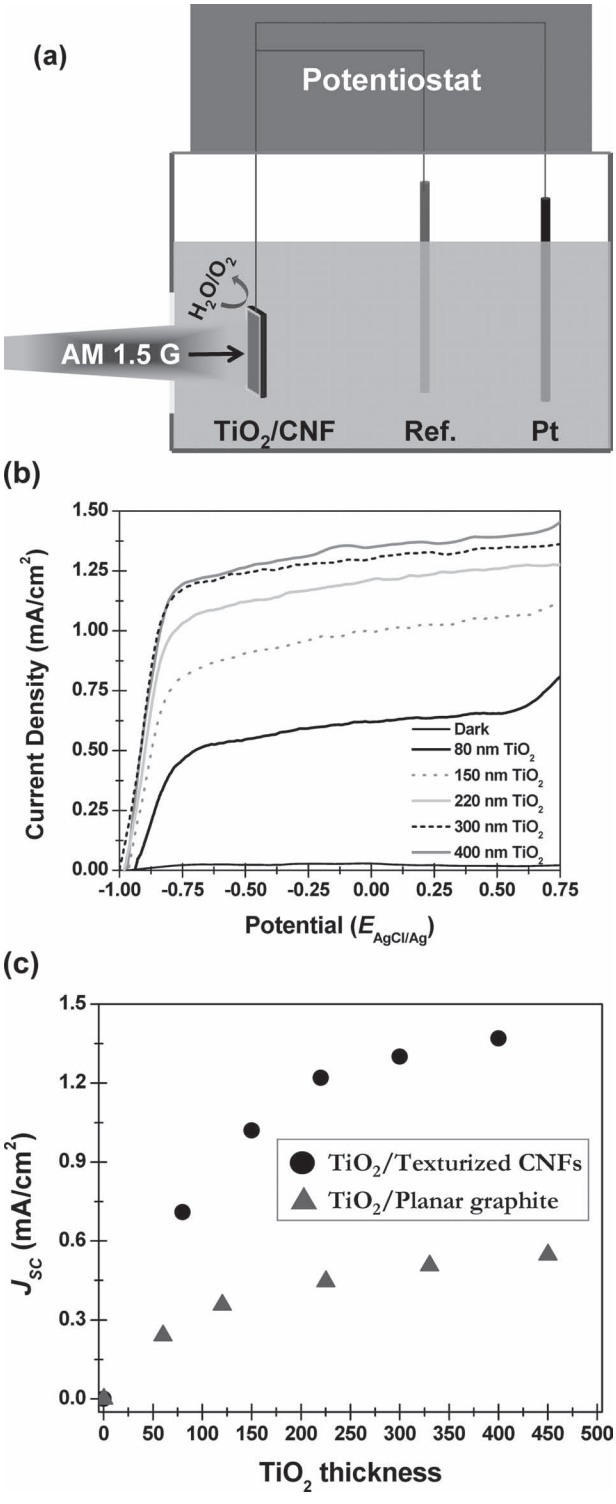

Figure 3. (a) Scheme depicting the three-electrode setup utilizing TiO_2 deposited on conductive CNF back contacts as the absorber of AM 1.5 G solar irradiation, and the reference (AgCl/Ag) and counterelectrode (Pt) configuration. (b) Current-potential curves of TiO_2 coated carbon nanofiber arrays with different TiO_2 thicknesses using a simulated AM 1.5 G solar spectrum in 1 M NaOH (dark current: 150 nm TiO_2/CNF) and (c) Short circuit current density (J_{SC}), defined at $E = 0.216$ V based on the three-electrode configuration, as a function of TiO_2 thickness for both TiO_2 coated, texturized CNFs and TiO_2 coated planar graphite.

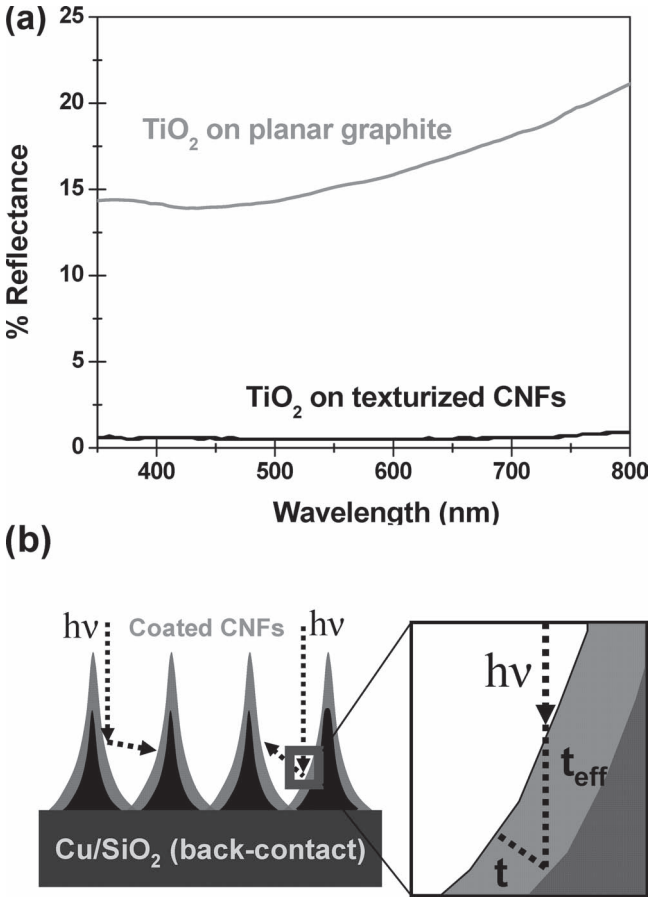

Figure 4. (a) Percent reflectance as a function of wavelength for both planar graphite and coated, texturized CNF arrays demonstrating the anti-reflective nature of the CNF arrays (60 and 80 nm TiO_2 coating, respectively). (b) Scheme depicting antireflective nature of highly 3-D structure, and visually demonstrating other possible means by which a 3-D structure can enhance behavior of a solar device.

ideal normal irradiation. Therefore, it should be used simply as a guideline rather than a strict calculation.

Experimental results in support of this geometric analysis are discussed in the supporting information (Figure S3), where similarly antireflective TiO_2/CNFs with a significantly lower pillar density (and lower out-of-plane angle) yield only a 2x enhancement to device performance in comparison to flat TiO_2/graphite. Although this does not decouple the physics of the absorption and collection processes that lead to these enhancements, it does demonstrate that electrode structure is a principle component of enhanced device performance from 3-D semiconductor scaffolds. Therefore, this suggests that the textured CNF electrodes as a back-contact for a thin semiconducting absorbing layer offers a rational approach for obtaining devices with a balance between the effective thickness for maximized absorption, and the actual thickness, which could ideally be tuned to L_D. In this particular case of TiO_2, this yields high efficiency since most absorbed photons have energies near the semiconductor band-gap energy. We further conclude that rational design of semiconductor architecture, in addition to chemical features of the semiconductor material (i.e. band

gap) are important in designing efficient solar devices. This is particularly true for metal-oxides, where poor minority carrier lifetimes can be compensated by tuning the structure of the electrode–perhaps yielding a route toward high efficiency devices from cheap and readily available materials.

In summary, we develop here a technique to fabricate scalable, 3D back-contact architectures for solar devices utilizing a solution-textured CNF array template. Utilizing TiO_2 as an example absorber layer for PEC, a ~3x enhancement of measured *J*SC was observed compared to planar substrates. We explain the enhancement as being due to a combination of reduced reflectance, enhanced absorption due to increased effective optical path length, and enhanced carrier collection efficiency. The CNF back-contacts reported here present a generic route for enhancing the performance of conventional thin-film solar devices, including PVs, especially for materials with small L_D, less than the characteristic absorption length. Graphitic CNFs are particularly attractive for such back-contact applications due to their high conductance, lack of surface native oxide layers, and high chemical robustness.

Experimental Section

Aligned Carbon Nanofiber Growth: Vertically aligned carbon nanofiber (CNF) arrays were grown in a plasma-enhanced chemical vapor deposition system utilizing C_2H_2, H_2, and NH_3 precursors using a general approach described in more detail elsewhere.[25] The as-grown samples had CNF vertical heights of ~10 μm based on SEM imaging. Catalyst growth substrates were deposited utilizing electron-beam evaporation using a 200 nm thick Cu layer, a 30 nm thick Ti layer, and a 30 nm thick Ni layer on a *p*-Si substrate with 50 nm SiO_2. The Ti layer acts as an interdiffusion barrier for the Ni catalyst while still allowing the substrate to remain conductive following growth. Following growth, the CNFs were exposed to liquid treatment using a drop of solvent, dried, and then coated using ALD.

Atomic Layer Deposition: ALD coating was performed using a Picosun Sunale system with intermittent 0.1 sec pulses of titanium tetrakis isopropoxide and water vapor between 5 second N_2 purges. The deposition temperature was 250 °C. This condition results in a deposition rate of ~0.2–0.3 Å/cycle.

AM 1.5 G Photocurrent Measurements: Photocurrent measurements were performed utilizing a Newport solar simulator (50–500 W, model 67005), which was tuned to 100 mW/cm^2 using a broadband power meter. The photocell in which measurements were performed was custom-made (Adams & Chittenden) with a 40 mm quartz window for sample illumination. Prior to filling the photocell with 1 M NaOH electrolyte, the incident light intensity was calibrated to 1 sun at the exact position where the TiO_2 absorbing material is illuminated. To compare the effect of electrode structure or TiO_2 thickness on measured photocurrents, current-potential curves are taken for different samples in the same configuration. To prepare electrodes for measurements, Ag paint is utilized to contact the Cu layer on which the 3-D carbon nanofibers are grown, and Dow Corning 3140 RTV waterproof adhesive is utilized to isolate all surfaces of the sample except the active TiO_2 coated CNFs.

Supporting Information

Supporting Information is available from the Wiley Online Library or from the author.

Acknowledgements

This work was partially funded by Berkeley Sensor and Actuator Center, and Mohr Davidow Ventures. The synthesis part of this work was supported by a LDRD from Lawrence Berkeley National Laboratory (LBNL). Reflectance measurements were performed using facilities in the Electronic Materials Program, LBNL, which is supported by supported by the Director, Office of Science, Office of Basic Energy Sciences, Materials Sciences and Engineering Division, of the U.S. Department of Energy under Contract No. DE-AC02-05CH11231. A.J. acknowledges a Sloan Fellowship and support from the World Class University program at Sunchon National University.

Received: July 31, 2011
Revised: September 28, 2011
Published online: October 26, 2011

[1] N. S. Lewis, D. G. Nocera, *Proc. Natl. Acad. Sci.* **2006**, *103*, 15729.
[2] Z. Y. Fan, H. Razavi, J. W. Do, A. Moriwaki, O. Ergen, Y. L. Chueh, P. W. Leu, J. C. Ho, T. Takahashi, L. A. Reichertz, S. Neale, K. Yu, M. Wu, J. W. Ager, A. Javey, *Nat. Mater.* **2009**, *8*, 648.
[3] P. V. Kamat, *J. Phys. Chem. C* **2007**, *111*, 2834.
[4] H. A. Atwater, A. Polman, *Nat. Mater.* **2010**, *9*, 205.
[5] Z. Y. Fan, R. Kapadia, P. W. Leu, X. B. Zhang, Y. L. Chueh, K. Takei, K. Yu, A. Jamshidi, A. A. Rathore, D. J. Ruebusch, M. Wu, A. Javey, *Nano Lett.* **2010**, *10*, 3823.
[6] Y. F. Huang, S. Chattopadhyay, Y. J. Jen, C. Y. Peng, T. A. Liu, Y. K. Hsu, C. L. Pan, H. C. Lo, C. H. Hsu, Y. H. Chang, C. S. Lee, K. H. Chen, L. C. Chen, *Nat. Nanotechnol.* **2007**, *2*, 770.
[7] R. Kapadia, Z. Y. Fan, A. Javey, *Appl. Phys. Lett.* **2010**, *96*, 103116.
[8] Y. J. Lin, G. B. Yuan, R. Liu, S. Zhou, S. W. Sheehan, D. W. Wang, *Chem, Phys. Lett.* **2011**, *507*, 209.
[9] M. De Volder, S. H. Tawfick, S. J. Park, D. Copic, Z. Z. Zhao, W. Lu, A. J. Hart, *Adv. Mater.* **2010**, *22*, 4384.
[10] S. Tawfick, M. De Volder, A. J. Hart, *Langmuir* **2011**, *27*, 6389.
[11] Z. Z. Zhao, S. H. Tawfick, S. J. Park, M. De Volder, A. J. Hart, W. Lu, *Physical Review E* **2010**, *82*, 041605.
[12] D. Eder, A. H. Windle, *Advanced Materials* **2008**, *20*, 1787.
[13] D. Eder, A. H. Windle, *Journal of Materials Chemistry* **2008**, *18*, 2036.
[14] G. J. Wang, M. W. Lee, Y. H. Chen, *Photochemistry and Photobiology* **2008**, *84*, 1493.
[15] Y. Yao, G. Li, S. Ciston, R. M. Lueptow, K. A. Gray, *Environmental Science & Technology* **2008**, *42*, 4952.
[16] H. T. Yu, X. Quan, S. Chen, H. M. Zhao, *Journal of Physical Chemistry C* **2007**, *111*, 12987.
[17] H. T. Yu, X. Quan, S. Chen, H. M. Zhao, Y. B. Zhang, *Journal of Photochemistry and Photobiology a-Chemistry* **2008**, *200*, 301.
[18] J. H. Bang, P. V. Kamat, *Adv. Funct. Mater.* **2010**, *20*, 1970.
[19] M. Z. Liu, N. D. Snapp,H. Park, *Chem. Sci.* **2011**, *2*, 80.
[20] G. K. Mor, K. Shankar, M. Paulose, O. K. Varghese, C. A. Grimes, *Nano Lett.* **2005**, *5*, 191.
[21] K. Shankar, J. I. Basham, N. K. Allam, O. K. Varghese, G. K. Mor, X. J. Feng, M. Paulose, J. A. Seabold, K. S. Choi, C. A. Grimes, *J. Phys. Chem. C* **2009**, *113*, 6327.
[22] O. K. Varghese, C. A. Grimes, *Sol. Energ. Mater. Sol. Cells* **2008**, *92*, 374.
[23] O. K. Varghese, M. Paulose, K. Shankar, G. K. Mor, C. A. Grimes, *J. Nanosci. Nanotechnol.* **2005**, *5*, 1158.
[24] T. Bak, J. Nowotny, M. Rekas, C. C. Sorrell, *Int. J. Hyd. Energ.* **2002**, *27*, 991.
[25] H. Ko, Z. X. Zhang, J. C. Ho, K. Takei, R. Kapadia, Y. L. Chueh, W. Z. Cao, B. A. Cruden, A. Javey, *Small* **2010**, *6*, 22.

[26] L. Miao, S. Tanemura,S. Toh, K. Kaneko,M. Tanemura, *J. Cryst. Growth* **2004**, *264*, 246.
[27] A. L. Linsebigler, G. Q. Lu, J. T. Yates, *Chem. Rev.* **1995**, *95*, 735.
[28] M. S. Dresselhaus, P. C. Eklund, *Advances in Physics* **2000**, *49*, 705.
[29] P. Salvador, *J. Appl. Phys.* **1984**, *55*, 2977.
[30] M. Takahashi, K. Tsukigi, T. Uchino, T. Yoko, *Thin Solid Films* **2001**, *388*, 231.
[31] K. R. Catchpole, A. Polman, *Appl. Phys. Lett.* **2008**, *93*, 191113.
[32] J. Y. Lee, P. Peumans, *Optics Express* **2010**, *18*, 10078.
[33] P. Matheu, S. H. Lim, D. Derkacs, C. McPheeters, E. T. Yu, *Appl. Phys. Lett.* **2008**, *93*, 113108.
[34] H. Tang, K. Prasad, R. Sanjines, P. E. Schmid, F. Levy, *J. Appl. Phys.* **1994**, *75*, 2042.